Attractive Ellipsoid Sliding Mode Observer Design for State of Charge Estimation of Lithium-Ion Cells

Anirudh Nath, *Member, IEEE*, Raghvendra Gupta, Rohit Mehta, Supreet Singh Bahga, Amit Gupta, and Shubhendu Bhasin, *Member, IEEE*

***Abstract*—This work investigates the real-time estimation of the state-of-charge (SoC) of Lithium-ion (Li-ion) cells for reliable, safe and efficient utilization. A novel attractive ellipsoid based sliding-mode observer (AESMO) algorithm is designed to estimate the SoC in real-time. The algorithm utilizes standard equivalent circuit model (ECM) of a Li-ion cell and provides reliable and efficient SoC estimate in the presence of bounded uncertainties in the battery parameters as well as exogenous disturbances. The theoretical framework of the observer design is not limited to the SoC estimation problem of Li-ion cell but applicable to a wider class of nonlinear systems with both matched and mismatched uncertainties. The main advantage of the proposed observer is to provide a fast and optimal SoC estimate based on minimization over the uncertainty bound. The proposed method is experimentally tested and evaluated for a range of temperatures using the hybrid pulse power characterization test (HPPC), EPA's Federal Test Procedure (FTP75) and Supplemental Test Procedure (US06) data, which demonstrate its effectiveness and feasibility.**

***Index Terms*—State-of-Charge (SoC), lithium-ion (Li-ion) cell, equivalent circuit model (ECM), sliding mode observers (SMO), attractive ellipsoid method AEM), linear matrix inequality (LMI).**

I. Introduction

LITHIUM-ION (Li-ion) cells are ubiquitous energy storage sources which provide a promising solution to the global future energy needs. In comparison to other battery technologies [1], [2], Li-ion cells offer several advantages such as excellent energy-to-weight ratio, no memory effect, and low self-discharge rate. All these favourable characteristics in conjunction with rapidly reducing costs have established Li-ion cells as the indispensable component for a wide variety of applications in the energy sector, especially in automotive, smart-grid and aerospace industries [3], [4].

Important issues associated with the use of Li-ion cells, including reliability, efficiency, and longevity, demand an efficient battery management system (BMS) capable of monitoring critical internal states of Li-ion cells such as the state of charge (SoC), state of health, energy density, etc. [3], [5], [6]. The SoC is a vital indicator of the actual amount of usable charge and energy content of the cell under operation, and requires monitoring to control the extent of charging and discharging to avoid overcharge or over-discharge. Due to nonlinear physics, it is not possible to directly measure SoC using external electrical signals and thus needs to be estimated. The simplest method for estimating the SoC is ampere-hour counting, an open-loop technique that requires precise knowledge of the initial SoC, which is typically not available and a poor initial guess often leads to accumulation of errors [7]. The open-circuit voltage (OCV) method is a simple procedure but not useful for online computation since it requires a long relaxation time for accurate and precise measurement of the OCV. Learning-based estimation methods, such as neural network and fuzzy logic [8]–[10], require extensive offline data for training and do not incorporate any information of the internal states of the cell. These techniques have drawbacks like overfitting, extensive training, difficult online adaptation, and high computational cost [7].

Model-based SoC estimation can be broadly classified into two main classes, namely, the filter-based estimation and the observer-based estimation techniques [11]. A summary of the various model-based SoC estimation algorithms, along with their limitations, is pictorially depicted in Fig. 1. KF based approaches have been extensively applied for SoC estimation [12]. The requirement of linear input-output relation leads to the nonlinear characteristic of the SoC-voltage relationship being lost, thereby limiting the effectiveness of this algorithm [13], [14]. The use of Taylor series in the extended Kalman filter (EKF) based approaches for linearization may often result in erroneous SoC estimation [14]–[16]. Linearization is avoided in unscented Kalman filter (UKF) based approaches [11], [17]. However, UKF based methods are sensitive to inaccuracies in the initial conditions and unknown disturbances [17]. The particle filtering methods can more effectively deal with the characteristics of the Li-ion cell but have its limitations as provided in Fig. 1 [12], [17]–[19].

Observer-based techniques can address limitations associated with the aforementioned filter-based SoC algorithms. Some of the most important works involve SoC estimation based on reduced-order observer technique [20], model reference adaptive observer [21], proportional-integral observer [22], unknown input observer [23] and nonlinear observers [24], [25]. Several observer-based algorithms are complicated due to the augmentation of online parameter identification based on SoC [20] that can

Manuscript received May 16, 2020; revised September 17, 2020; accepted October 12, 2020. Date of publication November 3, 2020; date of current version January 22, 2021. This work was supported by the Department of Science and Technology (DST) under Grant DST/TMD/MES/2K17/08(G). The review of this article was coordinated by Prof. M. Preindl. *(Corresponding author: Shubhendu Bhasin.)*

Anirudh Nath, Raghvendra Gupta, Rohit Mehta, Supreet Singh Bahga, and Amit Gupta are with the Department of Mechanical Engineering, Indian Institute of Technology Delhi, New Delhi 110016, India (e-mail: anirudh.nath88@gmail.com; raghvendrag6@gmail.com; rohit0149@gmail.com; bahga@mech.iitd.ac.in; agupta@mech.iitd.ac.in).

Shubhendu Bhasin is with the Department of Electrical Engineering, Indian Institute of Technology Delhi, New Delhi 110016, India (e-mail: sbhasin@ee.iitd.ac.in).

Digital Object Identifier 10.1109/TVT.2020.3035681

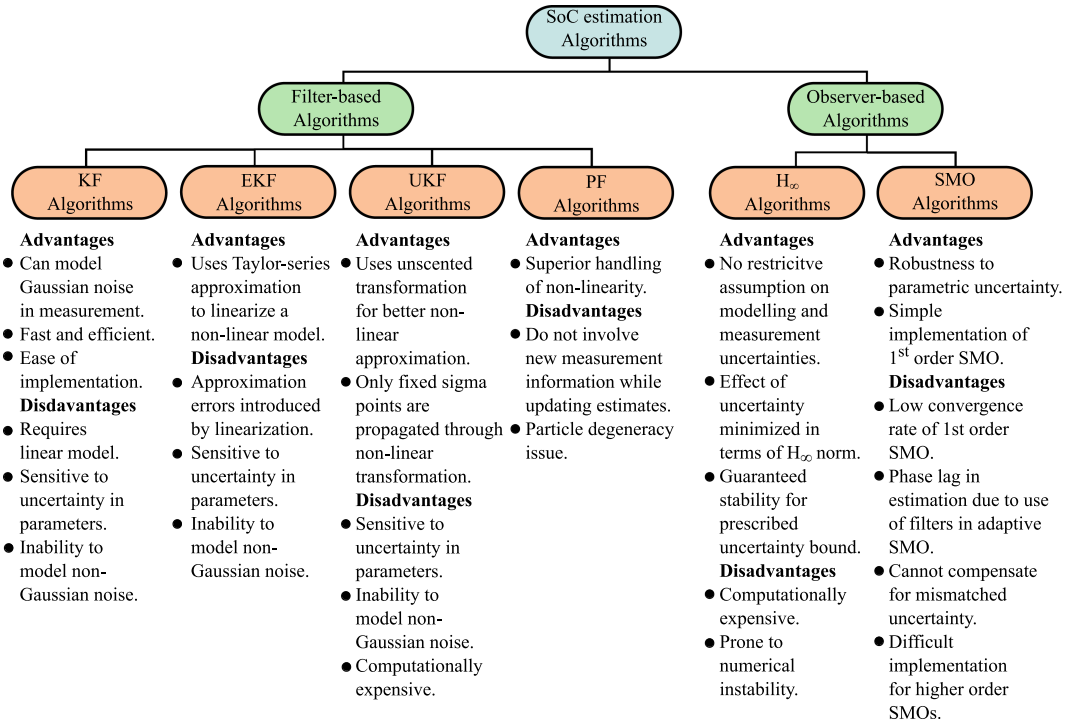

Fig. 1. Various filter-based and observer-based SoC estimation approaches.

be affected by external factors such as temperature and ageing effects [12]. Robust observer-based SoC algorithms, such as H_∞ filtering technique [26], [27] and sliding mode observer (SMO) methods [28], that utilize simplistic mathematical models of the Li-ion cell and information about the uncertainty bounds are designed to address these issues. As shown in Fig. 1, H_∞ filter-based SoC estimation algorithms are robust to modelling inaccuracies and bounded disturbances, but demand high computational power and implementation cost [12].

The SMO-based algorithms can be classified as (i) constant [29]–[32] and adaptive (time-varying) switching gain [29], [33] and (ii) first-order [30], [31], [33], [34] or second-order (based on the order of state equations) [35], [36], as discussed in [29]. While first-order SMOs are simple in their design and implementation [30], [33], [34] the second-order SMOs, have been shown to have higher accuracy in SoC estimation [35], [36]. Similarly, an adaptive SMO with time-varying switching gain provides superior performance as compared to their constant gain counterpart. However, in addition to the implementation of this algorithm being difficult, the use of low-pass filters further adds to the complexity, and the implementation cost [29]. Furthermore, the adaptive SMO based SoC estimation can be poor due to the phase lag introduced by the use of filters.

The attractive ellipsoid method presents an efficient, robust control strategy based on the invariant ellipsoid method in the numerically efficient linear matrix inequality (LMI) framework [37]. This technique has been applied in a wide range of applications ranging from robotics [38] to biomedical engineering [39]–[41]. The main motivation behind the current work is to propose a robust observer-based SoC estimation algorithm that can address the problems of the existing filter-based and observer-based approaches. Here a novel first-order SMO is proposed which utilizes a simple equivalent circuit model (ECM) of the Li-ion cells with fast convergence and avoids the limitations of existing adaptive SMOs. In general, the SMO [42] applied to a system with uncertainties should satisfy the matching condition, which ensures that the sliding motion is independent of the exogenous perturbations. In [43], the SMO design mainly concentrates on the robustness issues due to varying parameters, linearization, and the measurement noise. In the proposed method, we have incorporated the notion of robustness and optimality in the design. Further, unlike [43], prior information of the bound of the state estimation errors is not required. The SMO in [43] does not address the mismatched uncertainty present in the system, whereas the proposed attractive ellipsoid sliding mode observer (AESMO) addresses both matched and mismatched uncertainties in its formulation.

The main theoretical contribution of the proposed AESMO is that this design applies to a broad class of uncertain nonlinear affine systems with uncertainties that do not require the matching condition. Unlike conventional SMO, the current observer design does not require the matching condition. This method ensures a guaranteed convergence of SoC estimation error trajectories to a bounded ellipsoid of a minimal size where the observer gain matrix is obtained by solving a convex optimization problem with LMI constraints. It also avoids the requirement of high-end computational resources for its implementation, unlike the H_∞ and Kalman filter-based algorithms. Another essential feature of this design is that the rate of convergence of the estimated trajectories can be altered by adjusting the value of a design parameter. Thus the issue of slow convergence of existing first-order SMOs can be improved.

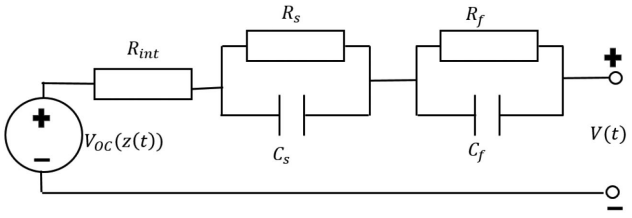

Fig. 2. Block diagram representation of the equivalent circuit model of Li-ion cell.

II. Mathematical Modelling of Li-Ion Cell

A. Equivalent Circuit Model of Li-ion Cell

Here, an ECM with dual-polarization RC circuit is considered for the purpose of SOC estimation. The ECM provides a good trade-off between complexities and precision of the electrical behaviour of the Li-ion cell [3]. Various versions of ECM models exist in the literature as mentioned in [4], [16], [26], [28], [44]. The presented observer design can accommodate modelling errors and parametric uncertainties. A schematic of the Li-ion ECM is shown in Fig. 2, where R_{int} is the internal ohmic resistance of the Li-ion cell. The RC networks (R_s, C_s) and (R_f, C_f) are, respectively, used to describe the short-term as well as long-term transient behaviour of the Li-ion cell. The mathematical relationship of the terminal voltage of the Li-ion cell which is expressed as linear sum of the OCV ($V_{\rm oc}$), the voltage drops across the internal resistance as well as the RC-modules (i.e., $R_{int}I(t)$, $V_{RC_1}(t)$ and $V_{RC_2}(t)$, respectively) are given as

$$V(t) = V_{\rm oc}(\mathrm{z}(t)) - V_{RC_1}(t) - V_{RC_2}(t) - R_{int}I(t) \tag{1}$$

The voltage drops across the RC modules representing the slow and fast polarization characteristics of the Li-ion cell, respectively, are given by

$$\dot{V}_{RC_1}(t) = -\frac{1}{R_sC_s}V_{RC_1}(t) + \frac{1}{C_s}I(t) \tag{2}$$

$$\dot{V}_{RC_2}(t) = -\frac{1}{R_fC_f}V_{RC_2}(t) + \frac{1}{C_f}I(t) \tag{3}$$

The SoC of Li-ion cell, $z(t)$ is related to the current and the nominal capacity of the Li-ion cell as follows:

$$\dot{z}(t) = -\frac{1}{Q}I(t) \tag{4}$$

where Q denotes the total capacity of the cell. The SoC can be expressed in terms of the terminal voltages and other voltage drops by substituting the expression for the current, $I(t)$ from (1) in (4) as

$$\dot{z}(t) = -\frac{1}{R_{int}Q}\left(V_{\rm OC}(z(t)) - V_{RC_1}(t) - V_{RC_2}(t) - V(t)\right) \tag{5}$$

Differentiating the terminal voltage, $V(t)$ with respect to time and assuming negligible change in current in between the sampling instants (i.e. $\frac{dI(t)}{dt} \simeq 0$) as in [12] and further utilizing (2) and (3), one can obtain

$$\begin{aligned}\dot{V}(t) &= \dot{z}\frac{\partial V_{\rm OC}(\mathrm{z})}{\partial z} - \dot{V}_{RC_2} - \dot{V}_{RC_1} - R_{int}\frac{dI}{dt}\\ &= -\frac{I}{Q}\frac{\partial V_{\rm OC}(\mathrm{z})}{\partial z} + \frac{1}{R_fC_f}V_{RC_2} - \frac{I}{C_f}\\ &\quad + \frac{1}{R_sC_s}V_{RC_1} - \frac{I}{C_s}\end{aligned} \tag{6}$$

Now all the dynamical equations described above can be summarised as follows

$$\begin{aligned}\dot{V} &= a_2V_{OC}(z) - a_2V + (a_3 - a_2)V_{RC_2}\\ &\quad - \left[b_1 \times \frac{dV_{\rm OC}(\mathrm{z})}{dz} + b_2 + b_3 - a_2R_{int}\right]I\\ \dot{z} &= -b_1\bar{R}\left(V_{\rm OC}(\mathrm{z}) - V - V_{RC_1} - V_{RC_2}\right)\\ \dot{V}_{RC_1} &= -a_2V_{RC_1} + b_2I\\ \dot{V}_{RC_2} &= -a_3V_{RC_2} + b_3I\end{aligned} \tag{7}$$

where $a_2 \triangleq \frac{1}{R_sC_s}, a_3 \triangleq \frac{1}{R_fC_f}, b_1 \triangleq \frac{1}{Q}, b_2 \triangleq \frac{1}{C_s}, b_3 \triangleq \frac{1}{C_f}$ and $\bar{R} \triangleq \frac{1}{R_{int}}$. The dynamical equations in (7) can be expressed as

$$\dot{x}(t) = (A + \Delta A(t))x(t) + Bu(t) + \phi(x(t), u(t)) + Dd(t) \tag{8}$$

and the output equation as

$$y(t) = Cx(t), \;\; y \in \mathbb{R} \tag{9}$$

where the state $x(t) \triangleq [V(t)z(t)V_{RC_1}(t)V_{RC_2}(t)]^T \in \mathbb{R}^4$, input $u(t) \triangleq I(t) \in \mathbb{R}$, exogenous disturbance $d(t) \in \mathbb{R}$,

$$A \triangleq \begin{bmatrix} -a_2 & a_2p_1 & 0 & a_3 - a_2\\ -b_1\bar{R} & -p_1b_1\bar{R} & -b_1\bar{R} & -b_1\bar{R}\\ 0 & 0 & -a_2 & 0\\ 0 & 0 & 0 & -a_3\end{bmatrix},$$

$$B \triangleq \begin{bmatrix} -b_2 - b_3 + a_2R_{int}\\ 0\\ b_2\\ b_3\end{bmatrix}, C = [1\,0\,0\,0],$$

$$\phi \triangleq \begin{bmatrix} a_2V_{OC}(z) - a_2p_1z - b_1\frac{\partial V_{\rm OC}(\mathrm{z})}{\partial z}I\\ -b_1\bar{R}V_{OC}(z) + p_1b_1\bar{R}z\\ 0\\ 0\end{bmatrix} \text{ and}$$

$$D \triangleq [1\;1\;1\;1]^T.$$

The system matrix in (8) is partitioned into a nominal matrix, A and an uncertain matrix,

$$\Delta A(t) = \begin{bmatrix} -\Delta a_2 & \Delta a_2p_1 & 0 & \Delta a_3 - \Delta a_2\\ -b_1\Delta\bar{R} & -p_1b_1\Delta\bar{R} & -b_1\Delta\bar{R} & -b_1\Delta\bar{R}\\ 0 & 0 & -\Delta a_2 & 0\\ 0 & 0 & 0 & -\Delta a_3\end{bmatrix}.$$

The elements of $\Delta A(t)$ vary within a specified interval $a_2 \in [a_{2_{\min}}, a_{2_{\max}}], a_3 \in [a_{3_{\min}}, a_{3_{\max}}]$ and $\Delta\bar{R} \in [\Delta\bar{R}_{\min}, \Delta\bar{R}_{\max}]$, where $a_{2_{\min}}$, $a_{3_{\min}}$, $\Delta\bar{R}_{\min}$ and $a_{2_{\max}}$, $a_{3_{\max}}$, $\Delta\bar{R}_{\max}$, respectively, are the known minimum and maximum values of the uncertain parameters.

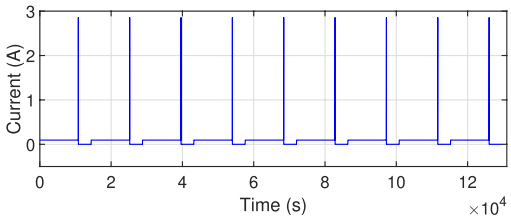

Fig. 3. Current profile for pulse discharge test utilized for parameter identification.

TABLE I
IMPORTANT VARIABLES AND ABBREVIATIONS

Symbol	Description
R_{int}	Internal resistance of the cell
R_s	Resistance (slow electrode dynamics)
C_s	Capacitance (slow electrode dynamics)
R_f	Resistance (fast electrode dynamics)
C_f	Capacitance (fast electrode dynamics)
z	State of charge(SoC) of the cell
$V_{oc}(z)$	Open circuit voltage of the cell
Q	Discharge capacity of the cell
p_i	i^{th} coefficient of polynomial fit
$\|\|\ .\ \|\|$	Eucledian norm
lim sup	Limit supremum
tr(.)	Trace operator
$(.)^T$	Transpose operator
e	Exponential function
$(.)^{-1}$	Inverse operator
LMI	Linear matrix inequality
SDP	Semi-definite programming
diag(a,b,...)	Diagonal matrix with diagonal enteries a,b,...
MAE	Mean absolute error
IAE	Integral absolute error
ISE	Integral square error
CCM	Coulomb counting method
UKF	Unscented Kalman filter
AESMO	Attractive ellipsoid sliding mode observer

B. Parameter Estimation

In the present work, the influence of ambient temperature has been taken into account. Hence, it is assumed that the values of R_{int}, R_s, C_s, R_f and C_f are dependent on SoC and temperature. For simplicity, the ECM parameters are assumed to be independent of the current direction (i.e. any hysteresis during charging and discharging is ignored).

The determination of the parameters has been carried out at 15 °C, 25 °C and 35 °C and the discharging current profile employed is shown in Fig. 3. For this purpose, Samsung INR18650-29E Li-ion cells with a nominal capacity of 2.85 Ah and Arbin LBT21084 Battery Cycler are used. The experimental profile of the input current consists of a 100 mA discharge current from 100% SoC (fully charged) till the time the SoC is 90%. After this, a pulse of 2.85 A current is applied for 10s followed by the rest of 4410s. This cycle is repeated for each step until the SoC drops to 10% as depicted in Fig. 3. The parameter identification procedure [45] utilizes nonlinear least-squares algorithm to determine the ECM parameters by using the experimental data of the applied current and corresponding terminal voltage of the Li-ion cell. The results of the estimated ECM parameters are provided in Table II.

An accurate mathematical relationship between the OCV and SoC is vital for the estimation accuracy since it captures the nonlinear dynamics of the Li-ion cell. The SoC versus OCV relationship was determined at temperatures of 15 °C, 25 °C and 35 °C using the voltage versus time data obtained by discharging the cell from an SoC of 1 to an SoC of 0 at C/30 rate. The SoC values at the temperature of 25 °C were taken to be 100% at 4.2 V and 0% at 3 V, and coulomb counting method (CCM) determined the intermediate SoC values. The initial SOC=1 was achieved by charging the cell to 4.2 V at a current of C/30 followed by a constant voltage charging until the current dropped to C/100. The temperature dependence of the SoC-OCV relationship, as evident from the experimental result in Fig. 4(a), was not significant. In the current study, the SoC-OCV relationship at 25 °C is considered for further analysis. A 12th-order polynomial function is considered for representing the nonlinear relationship between the OCV and SoC using the least-squares technique [16] as

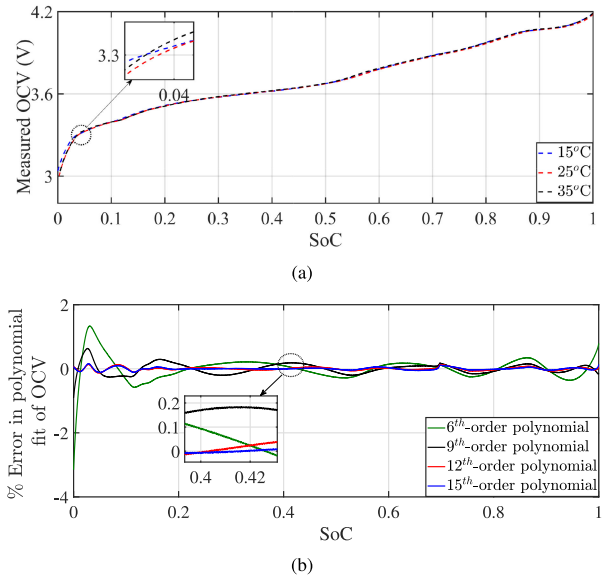

Fig. 4. Plots of (a) measured SoC-OCV curve at 15 °C, 25 °C and 35 °C; and (b) percentage error in fitting of the experimental SoC-OCV data using 6th, 9th, 12th and 15th degree polynomial functions.

$$V_{oc}(z) = \sum_{i=0}^{12} p_i z^i \tag{10}$$

where the coefficients of the function are identified as provided in Table III. The result of the polynomial function identification carried out at 25 °C is illustrated in Fig. 4(b) which shows the maximum absolute percentage error was observed to be 1.08% for a 9th-order fit and 0.22% for a 12th-order fit around the SoC value of 0. In addition, increasing the order of the polynomial fit any further does not result in any significant reduction in the error. The mean absolute error (MAE) and the root mean square error (RMSE) for the OCV-SoC fit for the 12th-order polynomial approximation are 0.0013 and 0.0017, respectively, which is comparable to recent literature, e.g., the MAE and RMSE of the OCV-SoC polynomial fitting in [46] are 0.0169 and 0.019, respectively.

III. Design of the Attractive Ellipsoid Based SMO Observer

In this section, a novel SMO design algorithm for a class of uncertain nonlinear Lipschitz systems as provided in (8)

TABLE II
PARAMETER IDENTIFICATION

SoC		0.1	0.2	0.3	0.4	0.5	0.6	0.7	0.8	0.9
R_{int} (Ω)	15°C	0.0518	0.0501	0.0495	0.0471	0.0469	0.0483	0.0387	0.0486	0.0481
	25°C	0.0401	0.0398	0.0395	0.0391	0.0387	0.0399	0.0402	0.0405	0.0400
	35°C	0.0330	0.0317	0.0314	0.0308	0.0307	0.0320	0.0321	0.0326	0.0319
R_s (Ω)	15°C	0.0265	0.0263	0.0285	0.0261	0.0268	0.0476	0.0287	0.0371	0.0252
	25°C	0.0186	0.0201	0.0226	0.0210	0.0202	0.0391	0.0371	0.0286	0.0207
	35°C	0.0148	0.0150	0.0179	0.0152	0.0129	0.0280	0.0241	0.0187	0.0135
R_f (Ω)	15°C	0.0253	0.0238	0.0210	0.0210	0.0201	0.007	0.0100	0.0115	0.0229
	25°C	0.0215	0.0197	0.0169	0.0181	0.0185	0.0008	0.0031	0.0119	0.0193
	35°C	0.0182	0.0167	0.0135	0.0156	0.0178	0.0040	0.0080	0.0139	0.0184
C_s ($\times 10^3$F)	15°C	1.3099	1.4717	1.4262	1.4648	1.4424	0.9778	1.0914	0.9414	1.3019
	25°C	1.6125	1.6529	1.6060	1.6363	1.6729	1.0902	0.9949	1.0949	1.5045
	35°C	1.8649	1.9431	1.9103	1.9614	2.1177	1.2512	1.2945	1.4097	1.8694
C_f ($\times 10^3$F)	15°C	2.4689	2.3514	2.4054	3.6231	4.0866	1.0785	3.3626	4.4072	5.5315
	25°C	3.3995	4.5190	2.4888	4.5317	4.9167	1.3658	3.6257	5.7759	7.1580
	35°C	3.4486	6.6375	2.7568	5.5145	7.1907	2.4570	5.6509	7.5140	7.9621

TABLE III
COEFFICIENTS AND RMSE FOR 12TH DEGREE POLYNOMIAL FIT FOR 15 °C, 25 °C AND 35 °C SOC-OCV DATA

Coefficients	15°C	25°C	35°C
p_0	3.035	2.950	2.955
p_1	1.479×10^1	1.861×10^1	1.872×10^1
p_2	-3.187×10^2	-3.857×10^2	-3.882×10^2
p_3	4.011×10^3	4.600×10^3	4.629×10^3
p_4	-3.015×10^4	-3.307×10^4	-3.344×10^4
p_5	1.447×10^5	1.531×10^5	1.562×10^5
p_6	-4.626×10^5	-4.754×10^5	-4.907×10^5
p_7	1.005×10^6	1.007×10^6	1.054×10^6
p_8	-1.488×10^6	-1.460×10^6	-1.549×10^6
p_9	1.477×10^6	1.420×10^6	1.530×10^6
p_{10}	-9.384×10^5	-8.861×10^5	-9.685×10^5
p_{11}	3.446×10^5	3.198×10^5	3.547×10^5
p_{12}	-5.563×10^4	-5.076×10^4	-5.713×10^4
RMSE	1.7×10^{-3}	1.6×10^{-3}	1.8×10^{-3}

is presented. The design procedure involves an appropriate selection of a sliding surface in the framework of the invariant ellipsoid method [41]. The proposed AESMO ensures that the state estimation error trajectories are ultimately confined within an attractive ellipsoidal set around the sliding manifold [38]. Based on the solutions to a convex optimization problem, appropriate observer gains are chosen to minimize the size of the attractive ellipsoid for a certain upper bound on the uncertainty while satisfying the stability conditions. The process of numerical computation of the observer gain is cast into an LMI framework, which provides a numerically tractable solution [38], [42]. Furthermore, the observer design involves an additional tunable design variable μ to improve the convergence time of the estimated SoC to the true SoC. Thus, the proposed algorithm ensures a robust estimate of the SoC with a high degree of accuracy in the presence of bounded uncertainties, such as modelling inaccuracies, the variability of system parameters with temperature and SoC, etc. Let us consider an observer with Luenberger's sliding mode structure (with the additional signum-term) as

$$\dot{\hat{x}}(t) = A\hat{x}(t) + Bu(t) + \phi(\hat{x}(t)) + L\sigma(t) + L_s SIGN(\sigma(t)) \tag{11}$$

where the output error is defined as

$$\sigma(t) \triangleq y(t) - C\hat{x}(t) = C\tilde{x}(t) \in \mathbb{R}^m, \tag{12}$$

the observer gain matrices, $L, L_s \in \mathbb{R}^{n\times m}$, the state estimate $\hat{x}(t) \in \mathbb{R}^n$ and the state estimation error defined as

$$\tilde{x}(t) \triangleq x(t) - \hat{x}(t) \in \mathbb{R}^n, \tag{13}$$

and $SIGN(\sigma) = [\text{sign}(\sigma_1), \text{sign}(\sigma_2), ..., \text{sign}(\sigma_m)]^T \in \mathbb{R}^m$ and the signum function $\text{sign}(\sigma_i)$ is defined as,

$$\text{sign}(\sigma_i) = \begin{cases} 1 & \text{if } \sigma_i > 0 \\ -1 & \text{if } \sigma_i < 0 \, i = 1, 2, \ldots, m \\ \in [-1, 1] & \text{if } \sigma_i = 0 \end{cases}$$

and $\sigma \in \mathbb{R}^m$ defines the sliding surface. Using (8) and (11), the closed-loop error dynamics can be written as

$$\begin{aligned} \dot{\tilde{x}}(t) = {} & A\tilde{x}(t) + \Delta A(t)x(t) + \Delta\phi \\ & - L\sigma(t) - L_s SIGN(\sigma(t)) + Dd(t) \end{aligned} \tag{14}$$

where $\Delta\phi \triangleq \phi(x(t)) - \phi(\hat{x}(t))$.

The following definition and lemma facilitate the subsequent design of a robust observer for the system in (7) in an LMI framework.

Definition: An ellipsoidal set $E(P_{attr}) \triangleq \{\tilde{x} | \tilde{x}^T P_{attr} \tilde{x} \leq 1\}$ where the ellipsoidal matrix P_{attr} is a symmetric positive definite matrix. $E(P_{attr})$ is called as an attractive ellipsoid for the system (14) if it is a globally asymptotic attractive invariant set [37].

Lemma III.1: A nonlinear mapping $\phi(x, u)$ is called Lipschitz function, if the following mathematical condition is satisfied,

$$\|\phi(x, u) - \phi(\hat{x}, u)\| \leq L_\phi \|x - \hat{x}\| \tag{15}$$

for any $(x, \hat{x}) \in \Re^n$ and $L_\phi > 0$ in (15) denotes a Lipschitz constant [39].

The following assumptions are considered for the observer design procedure.

Assumption 1: The states of (8) satisfy the mathematical inequality, $\|x(t)\| \leq X_+$ where X_+ is a known positive constant.

*Assumption 2:*The uncertain matrix is bounded, $\|\Delta A(t)\| \leq \gamma$. *Assumption 3:* The exogenous disturbance is also bounded as $\|d(t)\| \leq D_+$ where D_+ is a known positive constant.

Assumption 4: $\phi(x, u)$ in (8) satisfies the Lipschitz condition in Lemma 1.

Assumption 5: The pair (A,C) in (8) and (9) is observable [37].

Assumption 1 is a bounded input bounded output (BIBO) stability condition which is a practical consideration because the output, $V(t)$ of Li-ion cell can never be unbounded for a bounded input current, $I(t)$. The knowledge about various uncertainties can be determined based on experiments and domain knowledge. Thus Assumption 2 allows us to consider the effect of

measurement noise in the state and modelling inaccuracies separately in the observer design. Since the nonlinear map between $V_{OC}(z(t))$ and $z(t)$ is continuous and monotonic, Assumption 4 is also valid for the current problem and can be verified. The nonlinearity $\phi(x,u)$ in the system dynamics in (8) is composed of polynomial functions. It can be theoretically shown that the polynomial function satisfies the Lipshitz condition [47], where the Lipshitz constant depends on its coefficients.

Theorem III.2: For the system (8) satisfying the uncertainty bounds in Assumptions (1)–(4), if the observer (11) with gain $L_s = \frac{\mu}{2}P^{-1}C^T$ and observer gain matrix L fullfills the following matrix inequality,

$$\tilde{W}\left(P, L \mid \alpha, \varepsilon\right) = \begin{bmatrix} \Xi & P \\ P & -\varepsilon I_{n\times n} \end{bmatrix} < 0 \quad (16)$$

where

$$\Xi \triangleq P(A - LC + \frac{\alpha}{2}I_{n\times n}) + (A - LC + \frac{\alpha}{2}I_{n\times n})^T P + \varepsilon L_\phi^2 I_{n\times n},$$

for some positive definite symmetric matrix $P = P^T > 0$ and positive constants $\alpha > 0, \varepsilon > 0$ and $\mu > 0$, then the state estimation error $\tilde{x}(t)$ converges to a bounded region

$$\|\tilde{x}(t)\|^2 \leq \frac{1}{\lambda_{\min}(P)}\left(\frac{c}{\alpha} + O\left(e^{-\alpha t}\right)\right),$$

where $c \triangleq \varepsilon\gamma^2 X_+^2 + 4D_+^2$ and $O(e^{-\alpha t}) \triangleq \tilde{x}_0^T P \tilde{x}_0 e^{-\alpha t} - \frac{c}{\alpha}e^{-\alpha t}$, where $\tilde{x}_0$ is the initial estimation error.

Proof: Let us consider a Lyapunov candidate function

$$V(\tilde{x}) = \tilde{x}^T P \tilde{x} \quad (17)$$

where V is continuously differentiable, positive definite and radially unbounded and P is a symmetric positive definite matrix [37]. Taking the time derivative of (17) and using (14) yeilds

$$\dot{V}(\tilde{x}) = 2\tilde{x}^T P(A - LC)\tilde{x} + 2\tilde{x}^T P\left(\underbrace{\Delta A x + \Delta\phi + Dd(t)}_{\xi}\right) - 2\tilde{x}^T P L_s SIGN(\sigma) \quad (18)$$

Choosing $L_s = \frac{\mu}{2}P^{-1}C^T$ and using the relation $\sum_{i=1}^m |\sigma_i| \geq \|\sigma\|_2$, one can write

$$2\tilde{x}^T P L_s SIGN(\sigma) \geq \mu\|\sigma\| \quad (19)$$

Upper bounding (18) using (19)

$$\dot{V} \leq 2\tilde{x}^T P(A - LC)\tilde{x} + 2\tilde{x}^T P\xi - \mu\|\sigma\| \quad (20)$$

where $\xi \triangleq \Delta A x + \Delta\phi + Dd(t)$. Now, expressing (20) into symmetric form and adding and subtracting $\varepsilon I_{n\times n}$ and $\alpha V(\tilde{x})$ with scalars $\varepsilon, \alpha > 0$ on the left side of (18)

$$\dot{V}(\tilde{x}) = \begin{pmatrix} \tilde{x}(t) \\ \xi(t) \end{pmatrix}^T W \begin{pmatrix} \tilde{x}(t) \\ \xi(t) \end{pmatrix} + \varepsilon\|\xi\|^2 - \alpha V(\tilde{x}) - \mu\|\sigma\| \quad (21)$$

where $W \triangleq \begin{bmatrix} P(A - LC) + (A - LC)^T P + \alpha P & P \\ P & -\varepsilon I_{n\times n} \end{bmatrix}$. Now expanding $\|\xi\|^2 = \|\Delta A x + \Delta\phi + Dd(t)\|^2$ in (21) and using the bounds in Assumptions (1)–(4)

$$\begin{aligned} \|\xi\|^2 &= \|\Delta A x + \Delta\phi + Dd(t)\|^2 \\ &\leq \|\Delta A x\|^2 + \|\Delta\phi\|^2 + \|Dd(t)\|^2 \\ &\leq \gamma^2 X_+^2 + L_\phi^2\|\tilde{x}\|^2 + 4D_+^2 \end{aligned} \quad (22)$$

Substituting (22) in (21), we get

$$\dot{V}(\tilde{x}) \leq \begin{pmatrix} \tilde{x}(t) \\ \xi(t) \end{pmatrix}^T \underbrace{\begin{bmatrix} \Xi & P \\ P & -\varepsilon I_{n\times n} \end{bmatrix}}_{\tilde{W}(P, L|\alpha,\varepsilon)} \begin{pmatrix} \tilde{x}(t) \\ \xi(t) \end{pmatrix} - \alpha V(\tilde{x}) + \underbrace{\varepsilon\gamma^2 X_+^2 + 4D_+^2}_{c} - \mu\|\sigma\| \quad (23)$$

Now, if $\tilde{W}(P, L \mid \alpha, \varepsilon) < 0$, then from (23),

$$\dot{V}(\tilde{x}) \leq -\alpha V(\tilde{x}) + c - \mu\|\sigma\| \quad (24)$$

where $c > 0$ is a positive scalar constant that depends on the bounds on uncertainty. Equation (24) can be further upper bounded as

$$\dot{V}(\tilde{x}) \leq -\alpha V(\tilde{x}) + c \quad (25)$$

The solution of (25) can be obtained as

$$V(\tilde{x}) \leq V(\tilde{x}_0)e^{-\alpha t} + \frac{c}{\alpha}(1 - e^{-\alpha t}) \quad (26)$$

From (26), one can obtain

$$\limsup_{t\to\infty} V\left(\tilde{x}(t)\right) \leq \frac{c}{\alpha}. \quad (27)$$

Further (27) can be equivalently written as,

$$\limsup_{t\to\infty} \tilde{x}^T(t)\left[P_{attr}\right]\tilde{x}(t) \leq 1 \quad (28)$$

where $P_{attr} := \frac{\alpha}{c}P$ is the ellipsoidal matrix. Hence the stability of the state estimation error dynamics is proved since the time derivative of the storage function $V(\tilde{x})$ is uniformly ultimately bounded (UUB) under bounded uncertainty and disturbance.

It is to be worth mentioning at this stage that the size of $E(P_{attr})$ is minimized by solving a convex optimization problem with matrix constraints. Similar ideas have been used to compute an optimal observer gain matrix as in [39]–[41]. The minimization of the ellipsoidal set is presented in the corollary as provided below.

Corollary III.3: The optimal parameter L^* for the proposed observer is computed by solving a semidefinite programming problem (SDP) as follows:

$$\underset{P>0, L, \alpha>0, \varepsilon>0}{\text{minimize}} \; tr\left(P_{attr}\right) \quad (29)$$

where the operator $\mathrm{tr}(\cdot)$ represents the trace operator that is operated on the matrix P_{attr} satisfying the following matrix inequality,

$$\tilde{W}\left(P_{attr}, L \mid \alpha, \varepsilon\right) < 0 \quad (30)$$

The bilinear matrix inequality (BMI) in (30) is essentially nonlinear which needs to be converted to an LMI for solving the above convex optimization problem using standard LMI solvers.

Corollary III.4: The inequality in (30) can be converted to LMI if the first element of $\tilde{W}(P, L \mid \alpha, \varepsilon)$, i.e., Ξ is modified by introducing a new variable $Y \triangleq PL$ as follows:

$$\tilde{W}\left(P_{attr}, L^{*} \mid \alpha, \varepsilon\right) = \begin{bmatrix} \Xi & P \\ P & -\varepsilon I_{n\times n} \end{bmatrix} < 0,\ P > 0 \qquad (31)$$

where $\Xi = PA - YC + A^{T}P - Y^{T}P + \alpha P + \varepsilon L_{\phi}^{2} I_{n\times n}$ and the optimal observer gain matrix, L^{*} is computed as

$$L^{*} = P_{attr}^{*^{-1}} Y \qquad (32)$$

For fixed parameters, α and ε, the matrix inequalities presented in (31) become linear which can be solved using MATLAB toolboxes SeDuMi and YALMIP [48]. YALMIP and SeDuMi are standard solvers for semidefinite programming problems that involve LMI constraints [48]. YALMIP solver, that makes use of an external solver like SeDuMi to obtain a numerical solution of the optimization problem, is extensively used to solve optimization problems.

Remark 1: It can be noted that Corollary III.3 and Corollary III.4 are direct consequences of Theorem III.2 that makes use of some already established results in [37]–[39]. For instance, the idea of conversion of BMI into LMI by the change of variables is well established in the literature [37]. Similarly, the minimization of the attractive ellipsoid set by minimizing the trace of the ellipsoidal matrix, as presented in Corollary III.4 is presented in [39].

Remark 2: The novelty of the proposed AESMO in comparison with existing attractive ellipsoid-based SMO in [39]–[41], lies in its structure, which consists of an auxiliary design parameter μ that can be tuned to improve the convergence time of the estimated signals. Further, the observers in [39]–[41] lack the robustifying discontinuous term $L_{s}SIGN(\sigma(t))$ unlike the proposed observer in Eq. (11).

IV. Results and Discussion

In this section, experimental studies and numerical simulations are reported to validate and evaluate the proposed SoC estimation technique. At first, experimental validation of the real-time performance of the proposed AESMO is performed at 15 °C, 25 °C and 35 °C through HPPC, FTP75 and US06 tests. Next, several simulation scenarios are considered (i) to further investigate the robustness of the proposed AESMO with respect to uncertainty in parameters and random initial conditions, (ii) to compare its performance with an existing robust observer in [12] and the UKF in [11], (iii) to investigate the effect of measurement noise on the estimation performance of the AESMO and (iv) to establish the relationship between the design parameter μ and the convergence time of the estimated SoC to its true values. While conducting the experiments and simulations, the values of the model parameters in (8) are determined using linear interpolation from data given in Table II. The SDP problem in (29) with LMI constraints (31) is solved for $\mu = 10^{-10}$, $L_{\phi} = 0.8$, $\alpha = 2 \times 10^{7}$ and $\varepsilon = 2 \times 10^{-8}$. The solution of the SDP problem provided us with an optimal observer gain matrix, L with values $[0.3162 - 0.0898 - 1.4 \times 10^{-9} 0.0028]^{T}$, $[0.4019 - 0.2429 - 3.46 \times 10^{-9} 0.0053]^{T}$ and $[0.2915 - 0.1338 - 2.44 \times 10^{-9} 0.0029]^{T}$ at 15 °C, 25 °C and 35 °C, respectively.

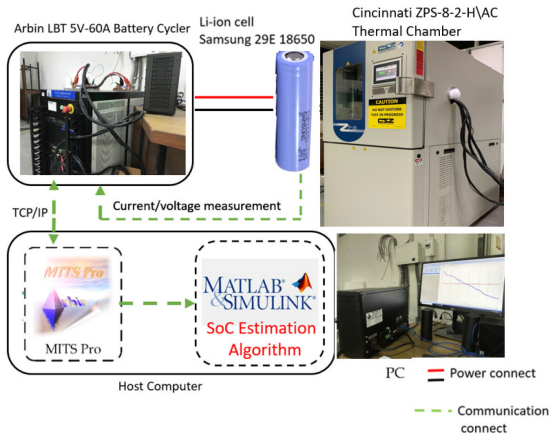

Fig. 5. Schematic diagram of the battery test bench.

A. Experimental Validation of the AESMO-Based SoC Estimation Algorithm

As shown in Fig. 5, Arbin LBT21084 5V-60A Battery Cycler along with Cincinnati Sub-Zero Thermal Chamber ZPS-8-2-H\AC is utilized to carry out experiments on the Li-ion cells. The experimental data are used to identify the ECM parameters of the cell at different temperatures, and quantify the efficacy of the proposed AESMO based SoC estimation technique. The resolution and accuracy of the voltage measurement of the Arbin LBT21084 5V-60A Battery Cycler are 2 μV and 0.02%, respectively. For the designed experiments, Li-ion cells INR18650-29E made by Samsung SDI Co., Ltd., are utilized having a nominal voltage and nominal capacity of 3.65 V and 2.85 Ah, respectively. The current and voltage measurement data are stored in the memory of the host computer with a sampling rate of 1 Hz. Finally, the recorded current and voltage data is imported to MATLAB/SIMULINK to be used in the SoC estimation algorithm.

Remark 3: In the current work, the CCM is considered as the benchmark for"true" SoC. This is a standard practice in literature [11] since the CCM is known to give reasonably accurate results if the initial SoC is exactly known, which is only possible in a controlled setting. The tests are done in a controlled setup which ensures that they begin from SoC=1.

Remark 4: The convergence time corresponds to the approximate time that the estimated SoC would take to reach within a $\pm 5\%$ band of the true SoC from an arbitrary initial condition after the start of the experiment.

The SoC estimation error, used to compute the MAE, integral absolute error (IAE) and integral square error (ISE),is obtained as the difference between the "true" SoC and the SoC estimate obtained from the estimation techniques, like the proposed AESMO, robust observer and UKF.

1) HPPC Test: The HPPC tests are conducted at different temperatures on the INR18650-29E cells and the proposed AESMO in (11) is utilized to estimate the SoC. The purpose of this experimental study is to investigate the real-time performance of the proposed AESMO in estimating the SoC from the arbitrary initial condition during the HPPC tests at different temperatures. Fig. 6(a)–(c) illustrates the estimation performance of the proposed AESMO during the HPPC tests. From Fig. 6(a)–(c), one can observe that despite the error in

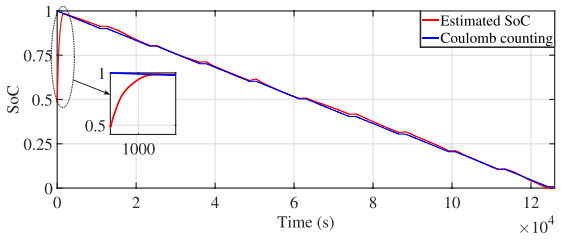

(a)

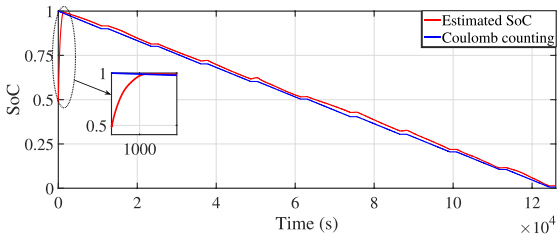

(b)

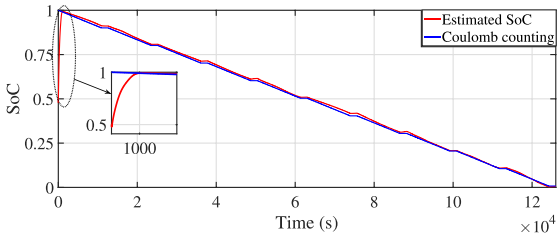

(c)

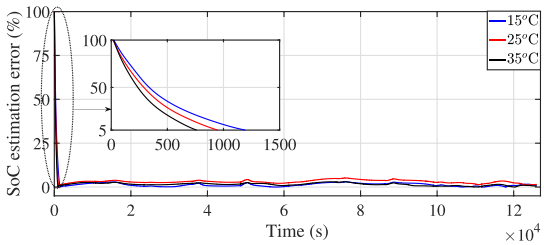

(d)

Fig. 6. Plot for SoC estimation results for HPPC test at (a) 15 °C, (b) 25 °C and (c) 35 °C, and (d) percentage errors in estimation.

TABLE IV
MAE AND CONVERGENCE TIME OF SOC ESTIMATION FOR HPPC, FTP75, AND US06 TESTS AT GIVEN TEMPERATURES

Temperature	FTP75		US06	
	MAE	Convergence time (s)	MAE	Convergence time (s)
15°C	0.0166	1201	0.0219	1205
25°C	0.0314	9675	0.0334	9665
35°C	0.0397	789	0.0338	799

initial SoC estimate ($z_0(t) = 0.5$), the proposed AESMO is able to estimate the experimental SoC for all the cases. The absolute percentage errors between the estimated SoC as provided by the AESMO and CCM at different temperatures are shown in Fig. 6(d). The corresponding MAE and convergence time for the SoC estimation at the three temperatures are given in Table IV. The percentage MAEs are restricted within 3.11% for all the cases.

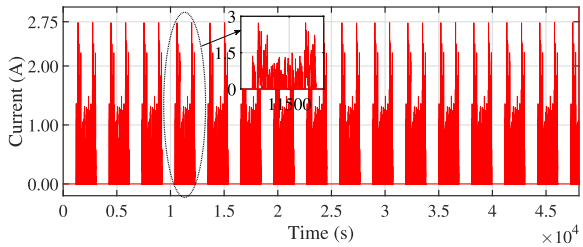

(a)

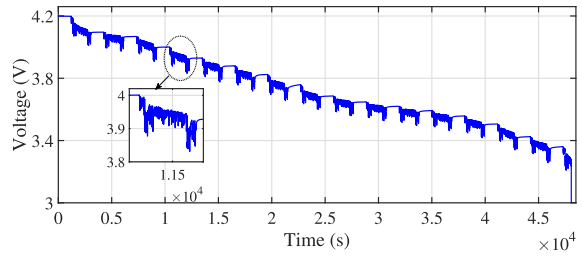

(b)

Fig. 7. Input current and terminal voltage of FTP75 test for the Li-ion cell at 15 °C.

2) FTP75 Test: In this case, the FTP75 driving cycle is considered to evaluate the estimation performance of the AESMO under dynamic loading conditions [49], [50]. The FTP75 is a standard drive cycle used in the United States for testing of light-duty vehicles. The test represents the transient driving behaviour with a large number of start-stops experienced while driving in cities. The cycle covers a distance of 17.77 km with an average speed of 34.12 km/h and a maximum speed 91.25 km/h in 1877 s [51]. An integrated current profile, comprising FTP75 drive cycle (1877 s) and rest (1800 s), is applied to the cell till the cell voltage drops below 3 V. The corresponding current and voltage profiles are depicted in Fig. 7(a) and (b), respectively. Since the ECM parameters are derived from an intermittent pulse-based current discharge profile, dynamic tests like the FTP75 experiment are useful in evaluating the effectiveness of the proposed method. The FTP75 test is conducted at the specified temperatures, and the corresponding results of the SoC estimation are shown in Fig. 8(a)–(c). It can be observed that despite an initial error of 0.5 in the SoC estimate, it converges to the true SoC. The corresponding percentage absolute errors between the estimated SoC and the true SoC are illustrated in Fig. 8(d). The MAE and the convergence time for the tests are provided in Table IV. It is observed that the percentage MAEs remain bounded within 3.97% of the true SoC.

3) US06 Test: In the third experimental study, the US06 drive cycle [49], [50], is considered.The driving cycle comprises a rapid acceleration and high-speed driving characteristics and is a representation of the driving on highways. The cycle covers a distance of 12.8 km with an average speed of 77.9 km/h and a maximum speed of 129.2 km/h in 596 s. The discharge current profile for the cell consists of the application of the US06 drive cycle of 576 s, followed with a rest 0f 1800 s till the cell voltage drops to 3 V. The dynamic current and the corresponding output voltage profiles for the US06 drive cycle are shown in Fig. 9(a) and (b), respectively. The experimental results of the US06 test at different temperatures are illustrated in Fig. 10.

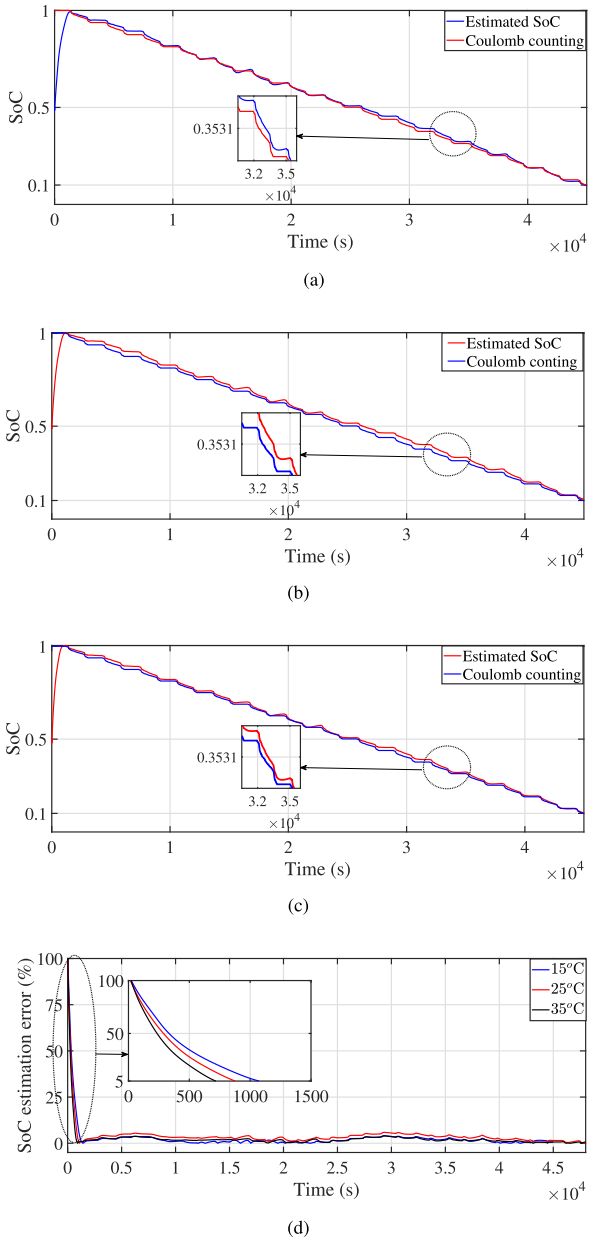

Fig. 8. Plot for SoC estimation results for FTP75 test at (a) 15 °C, (b) 25 °C and (c) 35 °C, and (d) percentage errors in estimation.

Fig. 10(a)–(c) illustrates that the estimated SoC converges to the true SoC from an initial value of 0.5. The corresponding percentage absolute errors are depicted in Fig. 10(d). Table IV illustrate the performance of the observer for the US06 tests in terms of MAE and convergence time. It should be noted that the percentage MAEs remain less than 3.38% of the true SoC.

4) Comparative Analysis: In this case, a comparative analysis of the estimation performance of the proposed AESMO with an existing robust observer [12] and UKF [11] is presented. The objective of this study is to investigate the performance of the above SoC estimation algorithms under highly fluctuating current. The simulations are carried out with nominal values of the ECM parameters for the US06 test at 35 °C as provided in

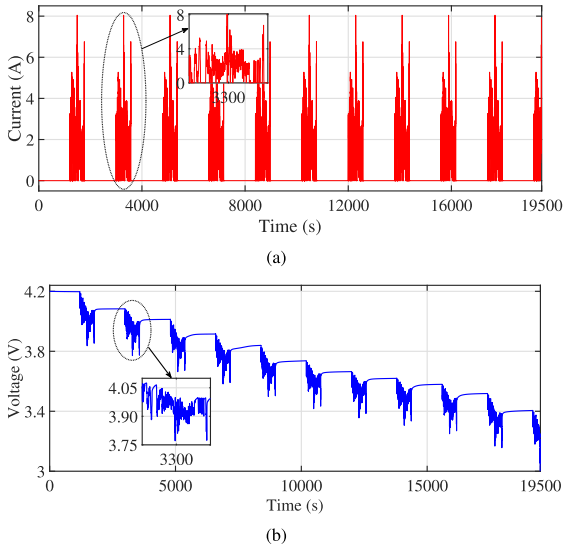

Fig. 9. Input current and terminal voltage of US06 test for the Li-ion cell at 15 °C.

Table II. The observer gain for the robust observer using the design method in [12] is computed as $L = [0.0197\ 0.0014\ 4.34 \times 10^{-5}\ 5.26 \times 10^{-5}]^T$. The parameters of UKF are considered as follows: (i) the initial covariance matrix as diag $(1 \times 10^{-8}, 5 \times 10^{-4}, 1 \times 10^{-8}, 1 \times 10^{-6})$, (ii) the additive process noise covariance as diag $(1 \times 10^{-1}, 1 \times 10^{-6}, 1 \times 10^{-4}, 1 \times 10^{-10})$, (iii) the additive measurement noise covariance as (1×10^{-4}) and (iv) the unscented transformation parameters as $\alpha = 1$, $\beta = 2$ and $\kappa = 0$.

Fig. 11(a) illustrates the temporal profile of the estimated SoC as provided by the AESMO, robust observer [12] and UKF. It can be observed that the time for the estimatated SoC to converge to its true value for the proposed AESMO, the robust observer and UKF is 830 s, 2210 s and 875 s, respectively. Hence, we conclude that the estimated SoC provided by the AESMO and UKF takes similar time to converge to the true SoC, while it takes significantly longer for the robust observer in [12]. The corresponding percentage absolute error between the estimated SoC and the true SoC for the above techniques are illustrated in Fig. 11(b). The MAE after convergence for the AESMO, the robust observer [12] and the UKF are 0.0171, 0.0152 and 0.0095, respectively. It can be observed that the MAE for the UKF is less than that of its observer counterparts. Theoretically, it is expected that the UKF will perform SoC estimation with a high degree of accuracy whenever precise information about the system (ECM parameters) is available. The robustness analysis with respect to the variation in parameters as well as the initial conditions for the above estimation techniques is presented in Section IV-B.

Remark 5: The above discussion reveals the fact that the performance of the AESMO, robust observer and UKF are similar in terms of the SoC estimation error for the nominal case after convergence. However, the convergence time of the AESMO is significantly less than its observer counterpart, which can be attributed to the tuning of the parameter μ, as explained in Scenario 3.

Remark 6: The UKF is the recursive algorithm where the old estimate is updated whenever new measurement information

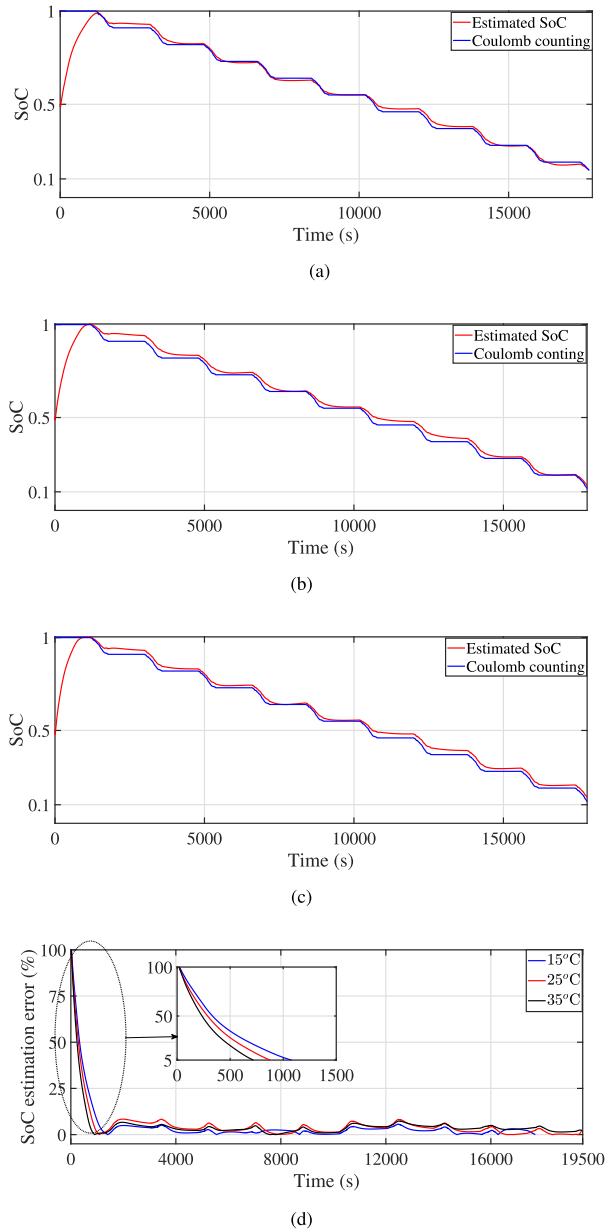

Fig. 10. Plot for SoC estimation results for US06 test at (a) 15 °C, (b) 25 °C and (c) 35 °C, and (d) percentage errors in estimation.

becomes available, which involves a series of computational steps - nonlinear unscented transformation, mean and covariance update and online computation of Kalman gains. The order of complexity of UKF is $O(N^3)$ [52]. The implementation of the proposed algorithm, on the other hand, consist of offline and online computation steps. The offline step, implemented once before the algorithm is run, involves computation computation of the optimal gain L^* through the solution of a semi-definite program, with the order of complexity $O(N^{3.5})$ [53]. However, the online step, computed whenever the new measurement information is obtained, involves the solution of Runge-Kutta numerical integration routine with a computational complexity of $O(N^2)$ [54]. Therefore, the running computational cost of the proposed algorithm is lower than that of UKF.

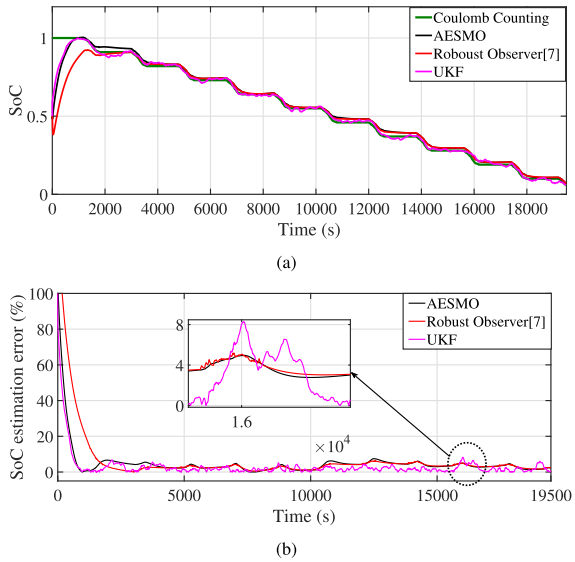

Fig. 11. Comparison between the SoC estimation for the US06 test at 35 °C between CCM, AESMO, robust observer [12] and UKF.

B. Simulation Scenarios

To further investigate the estimation performance of the AESMO, three additional simulation scenarios are considered. The first scenario contains robustness analysis of the proposed AESMO with an existing robust observer [12] and UKF [11]. The second scenario investigates the performance of AESMO in the presence of current and voltage measurement noise and the third one presents the effect of the observer design parameter μ on the convergence time of the estimated SoC to the true SoC. All the scenarios are explained in detail below.

1) Robustness Analysis of the AESMO With Existing SoC Estimation Algorithms: In this simulation scenario, a detailed robustness analysis of the proposed AESMO is done and compared with the robust observer in [12] and the UKF in [11]. In this robustness analysis, the performance of the estimation techniques are investigated with respect to a $\pm 30\%$ parametric uncertainty for US06 driving cycle at 15 °C, 25 °C and 35 °C. The initial condition of SoC is assumed to be unknown and is considered random ($0 \leq SoC \leq 1$) during the simulations. A total of 200 Monte Carlo simulations are carried out for each of the estimation techniques at different temperatures. It is worth mentioning that the observer parameters for the US06 test at a particular temperature are computed using the nominal values of the ECM parameters, as mentioned in Table II. The computed values of the observer parameters are then kept constant for all random simulations at that temperature. The parameters of the AESMO is chosen to be the same as Subsection 3 of Section IV. The observer gain for the robust observer using the design method in [12] is computed as $L = [0.0189\ 0.0017\ 3.87 \times 10^{-5}\ 3.75 \times 10^{-5}]^T$, $[0.0199\ 0.0014\ 4.52 \times 10^{-5}\ 4.90 \times 10^{-5}]^T$ and $[0.0197\ 0.0014\ 4.34 \times 10^{-5}\ 5.26 \times 10^{-5}]^T$ at 15 °C,25 °C and 35 °C, respectively. The parameters for the UKF is the same as mentioned in the previous case. It is important to note that the simulation setting is identical for all the above-mentioned SoC estimation techniques.

TABLE V
THE MEAN AND STANDARD DEVIATION (SD) OF THE ESTIMATION ERROR WITH THE PROPOSED AESMO, ROBUST OBSERVER [12] AND UKF AT 15 °C, 25 °C, AND 35 °C

SoC Estimation Technique	Temperature	MAE (± SD)	Mean ISE (± SD)	Mean IAE (± SD)
AESMO	15°C	0.0028 (±0.0021)	0.67 (±0.78)	118.73 (±75.02)
	25°C	0.0023 (±0.0016)	0.45 (±0.53)	101.63 (±69.51)
	35°C	0.0018 (±0.0015)	0.28 (±0.42)	78.17 (±52.55)
Robust Observer [7]	15°C	0.0090 (±0.0046)	1.68 (±1.87)	120.64 (±64.09)
	25°C	0.0065 (±0.0035)	1.08 (±1.06)	105.49 (±57.38)
	35°C	0.0048 (±0.0031)	0.65 (±0.68)	85.04 (±43.80)
UKF	15°C	0.0142 (±0.0121)	8.55 (±17.18)	232.84 (±75.02)
	25°C	0.0119 (±0.0093)	4.19 (±3.33)	200.65 (±90.10)
	35°C	0.0126 (±0.0111)	5.56 (±10.83)	199.99 (±103.80)

TABLE VI
STATISTICAL RESULT FOR THE PROPOSED AESMO UNDER THE EFFECT OF NOISE IN THE CURRENT AND VOLTAGE CHANNELS

MAE (± SD)	Mean ISE (± SD)	Mean IAE (± SD)
0.0014 (±.0017)	0.0905 (±1.0622)	25.90 (±.0053)

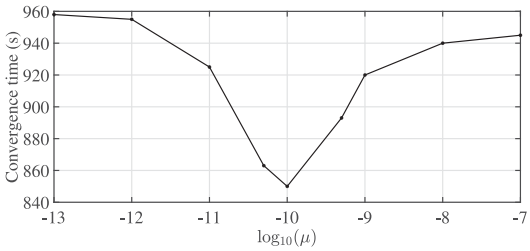

Fig. 12. Variation of convergence time with the design parameter μ.

The performance indices, MAE, mean ISE and mean IAE are computed for the random simulations for the AESMO, robust observer in [12] and the UKF in [11] at 15 °C, 25 °C and 35 °C, as provided in Table V. Further, from Table V the percentage reduction in the average values of the MAE of the AESMO with respect to the robust observer and the UKF at different temperatures are 65.67% and 82.17%, respectively. Thus, the proposed AESMO outperforms the robust observer and the UKF in terms of robustness to ±30% parametric uncertainty and random initial conditions. Referring to Table V, there is about 58.40% and 92.30% reduction in average values of the mean ISE of AESMO with respect to the robust observer and the UKF. In the same way, the percentage reduction in the average values of mean IAE for the AESMO with respect to the robust observer and the UKF are found to be 4% and 52.9%, respectively. The above discussion validates that the AESMO ensures a better SoC estimation as compared to the robust observer and the UKF, in the presence of ±30% parametric uncertainty.

2) Effect of Noise in Current and Voltage Measurements: This scenario considers the robustness of the AESMO concerning the presence of noisy signals in the current and voltage sensors. The current and voltage noise are assumed to be zero-mean Gaussian with variance 8% and 1%, respectively. With this setting, 200 Monte-Carlo simulations are carried out for the US06 test at 35 °C. Results are provided in Table VI.

3) Effect of the Design Parameter μ on the Convergence Time of the Estimated SoC: The following simulation study is designed to investigate the effect of the design parameter μ of the proposed observer on the convergence time of the estimated SoC. This investigation is done for the HPPC test at 25 °C. Fig. 12 illustrates the variation of the convergence time of the estimated SoC for different values of μ. It can be observed from Fig. 12 that at $\mu = 1 \times 10^{-10}$, the convergence time is about 850 s as compared to 960 s for $\mu = 1 \times 10^{-13}$. Thus, at $\mu = 1 \times 10^{-10}$, one can have about 11.46% reduction in the convergence time of the estimated SoC in contrast to $\mu = 1 \times 10^{-13}$. However, it is further increasing the value of μ results into increase in the convergence time. Therefore, it is possible to tune the value of μ to reduce the convergence time of the estimated SOC. This is an additional feature of the proposed AESMO as compared to other observers [12].

V. CONCLUSION

In this paper, attractive ellipsoid based SMO observer design has been proposed for Li-ion cells that provides robust estimates of the SoC in the presence of bounded parametric uncertainty, modelling inaccuracies and exogenous disturbance. The effect of temperature on the OCV-SoC relationship, ECM parameters and the SoC estimation performance of the proposed technique was investigated in an experimental setup. It has been reported that the proposed algorithm can provide reliable and fast SoC estimates as compared to UKF and robust observer [12] under uncertain conditions. Furthermore, a faster convergence rate of the estimated SoC was attained by tuning the design parameter μ. Due to its simplistic design, it can be easily implemented on low-cost devices. Extensive numerical simulations and experimental studies validate the capability of the proposed observer in estimating SoC in real-time in presence of noise in the current and voltage measurements, modelling inaccuracies and parametric variations.

Though only a single Li-ion cell has been considered, the extension of the proposed technique to the management of a battery pack can be an immediate future work. The accurate state estimation of battery packs is still an open problem due to inconsistent battery pack characteristics and uncertain operating conditions. The proposed technique can be augmented with the existing techniques, such as cell calculation, screening process, and bias correction methods for efficient state estimation of battery packs. As an immediate extension of the present work, the effect of ageing of the lithium-ion cells can be taken into consideration and validated experimentally. Furthermore, the effect of extreme low temperatures on the performance of the proposed method can also be explored. Apart from the ECM based methods, the proposed technique can be applied to physics-based models of Li-ion cells in the future.

REFERENCES

[1] J.-M. Tarascon and M. Armand, "Issues and challenges facing rechargeable lithium batteries," *Nature*, vol. 414, pp. 359–367, 2001.
[2] M. Armand and J.-M. Tarascon, "Building better batteries," *Nature*, vol. 451, pp. 652–657, 2008.
[3] H. Rahimi-Eichi, U. Ojha, F. Baronti, and M. Chow, "Battery management system: An overview of its application in the smart grid and electric vehicles," *IEEE Ind. Electron. Mag.*, vol. 7, no. 2, pp. 4–16, Jun. 2013.
[4] N. A. Chaturvedi, R. Klein, J. Christensen, J. Ahmed, and A. Kojic, "Algorithms for advanced battery-management systems," *IEEE Control Syst. Mag.*, vol. 30, no. 3, pp. 49–68, Jun. 2010.
[5] C. Zhang, L. Wang, X. Li, W. Chen, G. Yin, and J. Jiang, "Robust and adaptive estimation of state of charge for lithium-ion batteries," *IEEE Trans. Ind. Electron.*, vol. 62, no. 8, pp. 4948–4957, Aug. 2015.

[6] X. Hu, J. Jiang, D. Cao, and B. Egardt, "Battery health prognosis for electric vehicles using sample entropy and sparse bayesian predictive modeling," *IEEE Trans. Ind. Electron.*, vol. 63, no. 4, pp. 2645–2656, Apr. 2016.

[7] Z. Wei, C. Zou, F. Leng, B. H. Soong, and K. Tseng, "Online model identification and state-of-charge estimate for lithium-ion battery with a recursive total least squares-based observer," *IEEE Trans. Ind. Electron.*, vol. 65, no. 2, pp. 1336–1346, Feb. 2018.

[8] M. Charkhgard and M. Farrokhi, "State-of-charge estimation for lithium-ion batteries using neural networks and ekf," *IEEE Trans. Ind. Electron.*, vol. 57, no. 12, pp. 4178–4187, Dec. 2010.

[9] M. Shahriari and M. Farrokhi, "Online state-of-health estimation of VRLA batteries using state of charge," *IEEE Trans. Ind. Electron.*, vol. 60, no. 1, pp. 191–202, Jan. 2013.

[10] Y. Lee, W. Wang, and T. Kuo, "Soft computing for battery state-of-charge (BSOC) estimation in battery string systems," *IEEE Trans. Ind. Electron.*, vol. 55, no. 1, pp. 229–239, Jan. 2008.

[11] G. L. Plett, *Battery Management Systems, Volume II: Equivalent-Circuit Methods*. United States of America: Artech House, vol. 2, Dec. 2015.

[12] M. Gholizadeh and A. Yazdizadeh, "State of charge estimation of a lithium-ion battery using robust non-linear observer approach," *IET Elect. Syst. Transp.*, vol. 9, no. 1, pp. 1–7, Mar. 2019.

[13] B. Xia, C. Chen, Y. Tian, W. Sun, Z. Xu, and W. Zheng, "Battery management system: An overview of its application in the smart grid and electric vehicles," *J. Power Sources*, vol. 270, pp. 359–366, 2014.

[14] S. Gao, M. Kang, L. Li, and X. Liu, "Estimation of state-of-charge based on unscented kalman particle filter for storage lithium-ion battery," *J. Eng.*, vol. 2019, no. 16, pp. 1858–1863, 2019.

[15] J. Kim, S. Lee, and B. H. Cho, "Complementary cooperation algorithm based on dekf combined with pattern recognition for soc/capacity estimation and soh prediction," *IEEE Trans. Power Electron.*, vol. 27, no. 1, pp. 436–451, Jan. 2012.

[16] B. Haus and P. Mercorelli, "Polynomial augmented extended Kalman filter to estimate the state of charge of lithium-ion batteries," *IEEE Trans. Veh. Technol.*, vol. 69, no. 2, pp. 1452–1463, Feb. 2020.

[17] S. Gao, M. Kang, L. Li, and X. Liu, "Estimation of state-of-charge based on unscented kalman particle filter for storage lithium-ion battery," *J. Eng.*, vol. 2019, no. 16, pp. 1858–1863, 2019.

[18] Y. Wang, C. Zhang, and Z. Chen, "A method for state-of-charge estimation of lifepo4 batteries at dynamic currents and temperatures using particle filter," *J. Power Sources*, vol. 279, pp. 306–311, 2015.

[19] I.-S. Kim, "The novel state of charge estimation method for lithium battery using sliding mode observer," *J. Power Sources*, vol. 163, no. 1, pp. 584–590, 2006.

[20] H. Chaoui and P. Sicard, "Accurate state of charge (SOC) estimation for batteries using a reduced-order observer," in *Proc. IEEE Int. Conf. Ind. Technol.*, 2011, pp. 39–43.

[21] M. Verbrugge and E. Tate, "Adaptive state of charge algorithm for nickel metal hydride batteries including hysteresis phenomena," *J. Power Sources*, vol. 126, no. 1, pp. 36–249, 2004.

[22] J. Xu, C. C. Mi, B. Cao, J. Deng, Z. Chen, and S. Li, "The state of charge estimation of lithium-ion batteries based on a proportional-integral observer," *IEEE Trans. Veh. Technol.*, vol. 63, no. 4, pp. 1614–1621, 2014.

[23] D. C. Cambron and A. M. Cramer, "A lithium-ion battery current estimation technique using an unknown input observer," *IEEE Trans. Veh. Technol.*, vol. 66, no. 8, pp. 6707–6714, Aug. 2017.

[24] B. Xia, C. Chen, Y. Tian, W. Sun, Z. Xu, and W. Zheng, "A novel method for state of charge estimation of lithium-ion batteries using a nonlinear observer," *J. Power Sources*, vol. 270, pp. 359–366, 2014.

[25] M. El Lakkis, O. Sename, M. Corno, and D. Bresch Pietri, "Combined battery soc/soh estimation using a nonlinear adaptive observer," in *Proc. Eur. Control Conf.*, 2015, pp. 1522–1527.

[26] Q. Zhu, L. Li, N. Xiong, and G. Hu, "h_∞-based nonlinear observer design for state of charge estimation of lithium-ion battery with polynomial parameters," *IEEE Trans. Veh. Technol.*, vol. 66, no. 12, pp. 10 853–10 865, Dec. 2017.

[27] J. Wang, R. Xiong, L. Linlin, and Y. Fang, "A comparative analysis and validation for double-filters-based state of charge estimators using battery-in-the-loop approach," *Appl. Energy*, vol. 229, no. C, pp. 648–659, 2018.

[28] Y. Feng, C. Xue, Q. Han, F. Han, and J. Du, "Robust estimation for state-of-charge and state-of-health of lithium-ion batteries using integral-type terminal sliding-mode observers," *IEEE Trans. Ind. Electron.*, vol. 67, no. 5, pp. 4013–4023, May 2020.

[29] X. Sui, S. He, D. Stroe, X. Huang, J. Meng, and R. Teodorescu, "A review of sliding mode observers based on equivalent circuit model for battery soc estimation," in *Proc. IEEE 28th Int. Symp. Ind. Electron.*, 2019, pp. 1965–1970.

[30] B. Xiong, J. Zhao, Y. Su, Z. Wei, and M. Skyllas-Kazacos, "State of charge estimation of vanadium redox flow battery based on sliding mode observer and dynamic model including capacity fading factor," *IEEE Trans. Sustain. Energy*, vol. 8, no. 4, pp. 1658–1667, Oct. 2017.

[31] X. Chen, W. Shen, Z. Cao, and A. Kapoor, "Sliding mode observer for state of charge estimation based on battery equivalent circuit in electric vehicles," *Australian J. Elect. Electron. Eng.*, vol. 9, no. 3, pp. 225–234, 2012.

[32] M. Gholizadeh and F. R. Salmasi, "Estimation of state of charge, unknown nonlinearities, and state of health of a lithium-ion battery based on a comprehensive unobservable model," *IEEE Trans. Ind. Electronics*, vol. 61, no. 3, pp. 1335–1344, Mar. 2014.

[33] B. Ning, B. Cao, B. Wang, and Z. Zou, "Adaptive sliding mode observers for lithium-ion battery state estimation based on parameters identified online," *Energy*, vol. 153, no. C, pp. 732–742, 2018.

[34] Y. Shtessel, C. Edwards, L. Fridman, and A. Levant, *Sliding Mode Control and Observation*. Birkhäuser Basel, 2014.

[35] B. Ning, B. Cao, B. Wang, and Z. Zou, "Second-order discrete-time sliding mode observer for state of charge determination based on a dynamic resistance li-ion battery model," *Energies*, vol. 6, no. 10, 2013, Art. no. 55385551.

[36] Y. Huangfu, J. Xu, D. Zhao, Y. Liu, and F. Gao, "A novel battery state of charge estimation method based on a super-twisting sliding mode observer," *Energies*, vol. 11, no. 5, 2018, Art. no. 1211.

[37] A. Poznyak, A. Polyakov, and V. Azhmyakov, "Attractive ellipsoid method with adaptation," in *Attractive Ellipsoids in Robust Control. Systems & Control: Foundations & Applications*. Birkhäuser Cham, Aug. 2014.

[38] R. Falcon, H. Rios, M. Mera, and A. Dzul, "Attractive ellipsoid-based robust control for quadrotor tracking," *IEEE Trans. Ind. Electronics*, vol. 67, no. 9, pp. 7851–7860, Sep. 2020.

[39] A. Nath, D. Deb, and R. Dey, "Robust observer-based adaptive control of blood glucose in diabetic patients," *Int. J. Control*, 2020.

[40] A. Nath and R. Dey, "Robust guaranteed cost output feedback control of blood glucose in type 1 diabetes patient with intra-patient variability," *Optimal Control Appl. Methods*, pp. 1422–1438, 2020.

[41] A. Nath and R. Dey, "Robust observer based control for plasma glucose regulation in type 1 diabetes patient using attractive ellipsoid method," *IET Syst. Biol.*, vol. 13, no. 2, pp. 84–91, 2019.

[42] B. Sanchez, C. Cuvas, P. Ordaz, O. Santos-Sanchezl, and A. Poznyak, "Full-order observer for a class of nonlinear systems with unmatched uncertainties: Joint attractive ellipsoid and sliding mode concepts," *IEEE Trans. Ind. Electronics*, vol. 67, no. 7, pp. 5677–5686, Jul. 2020.

[43] J. Du, Z. Liu, Y. Wang, and C. Yen, "An adaptive sliding mode observer for lithium-ion battery state of charge and state of health estimation in electric vehicles," *Control Eng. Practice*, vol. 54, pp. 81–90, 2016.

[44] R. Xiong, J. Cao, Q. Yu, H. He, and F. Sun, "Critical review on the battery state of charge estimation methods for electric vehicles," *IEEE Access*, vol. 6, pp. 1832–1843, 2018.

[45] W. Li, L. Liang, W. Liu, and X. Wu, "State of charge estimation of lithium-ion batteries using a discrete-time nonlinear observer," *IEEE Trans. Ind. Electron.*, vol. 64, no. 11, pp. 8557–8565, Nov. 2017.

[46] F. Guo, G. Hu, P. Zhou, J. Hu, and Y. Sai, "State of charge estimation in electric vehicles at various ambient temperatures," *Int. J. Energy Res.*, vol. 44, no. 9, pp. 7357–7370, 2020.

[47] K. Eriksson, D. Estep, and C. Johnson, *Applied Mathematics Body and Soul: Vol I-III.*, Springer-Verlag Publishing, vol. 1, p. 3, 2003.

[48] J. Löfberg, "YALMIP : A toolbox for modeling and optimization in MATLAB," in *Proc. CACSD Conf.*, Taipei, Taiwan, 2004, pp. 284–289.

[49] J. X. Teoh, M. Stella, and K. W. Chew, "Performance analysis of electric vehicle in worldwide harmonized light vehicles test procedure via vehicle simulation models in advisor," in *Proc. IEEE 9th Int. Conf. Syst. Eng. Technol.*, 2019, pp. 215–220.

[50] Y. Tripathy, A. McGordon, and C. T. Low, "A new consideration for validating battery performance at low ambient temperatures," *Energies*, vol. 11, 2018.

[51] "Ftp-75," [Online]. Available: https://dieselnet.com/standards/cycles/ftp75.php

[52] S. Lu, L. Cai, Lu Ding, and J. Chen, "Two efficient implementation forms of unscented Kalman filter," in *Proc. IEEE Int. Conf. Control Autom.*, 2007, pp. 761–764.

[53] R. Masashi Fukuda and T. Abro, "Linear, quadratic, and semidefinite programming massive mimo detectors: Reliability and complexity," *IEEE Access*, vol. 7, pp. 29 506–29 519, 2019.

[54] R. M. Corless, "A new view of the computational complexity of IVP for ode," *Numerical Algorithms*, vol. 31, no. 1-4, pp. 115–124, 2002.